**SUPPLEMENTARY MATERIAL**

# Pyrolysis and co-combustion of semi-dry sewage sludge and bituminous coal: thermodynamics, kinetics and combustion characteristics

Guangyang Li[†], Zhuoyuan Chen[†], Afeng Wu[††], Tao Shi[††], Xiong Zhang[*, †], Hui Li[†††], Haiping Yang[†], Jingai Shao[†], Shihong Zhang[†], Hanping Chen[†]

†*State Key Laboratory of Coal Combustion, School of Energy and Power Engineering, Huazhong University of Science and Technology, 430074 Wuhan, PR China*

††*China Energy Engineering Group Guangdong Electric Power Design Institute Co., Ltd. 510663 Guangzhou, PR China*

†††*State Key Laboratory of Utilization of Woody Oil Resource, Hunan Academy of Forestry, 410004 Changsha, PR China*

∗Corresponding information:

Xiong Zhang; 1037 Luoyu Road, Wuhan, Hubei, P. R. China; Tel: +86-27-87542417; Fax: +86-27-87545526; Email: zhangxiong107@163.com.

## 1 The methods

### 1.1 Thermogravimetry analysis

Thermogravimetric analysis (TG) is a technical method to continuously measure the mass and temperature of the heated material under programmed temperature control conditions [1-3]. The TG experiments were conducted using a TG analyzer (Evo1150, Setaram, France), which can measure the quality change of samples in real-time under specific atmosphere and programmed temperature control conditions

to obtain the weight loss information such as dehydration, decomposition, and volatilization or weight gain information such as hydration, oxidation and adsorption.

To comprehensively evaluate the pyrolysis and combustion characteristics of sludge, the TG curve and data were analyzed in this study, and the following evaluation parameters were used [4]: maximum precipitation rate [$(dw_1/dt)_{max}$, %/min]; maximum precipitation temperature ($T_{1max}$, °C) corresponding to $(dw_1/dt)_{max}$; initial volatile temperature ($T_s$, °C) what is the inflection point temperature corresponding to the lowest point of the first curve after the loss of water on the curve; maximum volatile release rate [$(dw_2/dt)_{max}$, %/min]; temperature ($T_{2max}$, °C) corresponding to $(dw_2/dt)_{max}$; temperature ($\Delta T_{1/2}$, °C) corresponding to $(dw/dt)_{max})/(dw_2/dt)_{max} = 0.5$; final temperature residue ratio (R, %), 900°C as the final temperature of pyrolysis.

The larger the value of $(dw_2/dt)_{max}$, the more intense the release of volatiles, and the smaller the $T_s$, the easier the volatiles are precipitated. The smaller the $T_{2max}$, the narrower the $\Delta T_{1/2}$, the earlier and more concentrated the peak value of volatilization analysis, and the better the ignition characteristics and combustion efficiency of sludge.

Based on the above parameters, the volatile matter release characteristic index (D, $\%\cdot min^{-1}\cdot C^{-3}$) can be defined as follows:

$$D = \frac{(dw_2/dt)_{max}}{T_{2max} \times T_s \times \Delta T_{1/2}} \quad \text{(S1)}$$

The higher the value, the better the volatilization characteristics of sludge, and the easier the pyrolysis reaction.

**1.2 Combustion index**

To evaluate the combustion characteristics of SS more comprehensively, the TG data were analyzed. The following evaluation parameters were used [5,6]:

Ignition temperature $T_i$ is one of the indicators to evaluate the ignition performance of the fuel. It refers to the lowest temperature at which the fuel reaches continuous combustion. The lower the ignition temperature, the better the ignition performance. In this study, the TG-DTG method was used to determine the ignition temperature of samples, i.e., to find the peak point on the DTG curve as the intersection point between the vertical line and TG curve, then, to use the tangent plug-in to obtain a tangent line, and the intersection point between the tangent line and parallel line when weight loss begins is the $T_i$.

Burnout temperature $T_f$ refers to the burnout characteristics of fuel. The higher the $T_f$, the worse the burnout characteristics of fuel. In this study, the temperature corresponding to the weight-loss rate accounting for 95% of the total weight-loss rate was used as the $T_f$.

The maximum weight-loss rate $(dw/dt)_{max}$ represents the intensity of the reaction during combustion, and $T_{max}$ reflects the temperature at which the maximum weight-loss rate is achieved. The larger the max, the more intense the reaction. The smaller the $T_{max}$, the easier the sample will reach the $(dw/dt)_{max}$ and the easier the sample will burn. And the $(dw/dt)_{mean}$ reflects the mean combustion temperature.

Flammability index C reflects the speed of fuel combustion and the degree of difficulty in igniting. The larger the flammability index, the better the ignition stability of the sample [7]. It can be calculated as follows:

$$C = \frac{(\mathrm{dw}/\mathrm{dt})_{\max}}{T_{\mathrm{i}}^{2}} \quad \text{(S2)}$$

The flammability stability index G reflects the difficulty of fuel ignition and burnout. It can be calculated as follows:

$$G = \frac{(\mathrm{dw}/\mathrm{dt})_{\max}}{\mathrm{T}_{\max} \times \mathrm{T}_{\mathrm{i}}} \quad \text{(S3)}$$

The comprehensive combustion characteristic index S is a comprehensive index to evaluate the combustion characteristics of fuel. It can fully reflect the ignition and burnout performance of the sample. The larger the value of S, the better the overall combustion performance of the fuel. It can be calculated as follows:

$$S = \frac{(\mathrm{dw}/\mathrm{dt})_{\max}(\mathrm{dw}/\mathrm{d}t)_{\mathrm{mean}}}{T_{\mathrm{i}}^{2}T_{\mathrm{f}}} \quad \text{(S4)}$$

where the mean combustion rate $(dw/dt) = \beta(w_0 - w_1)/(T_F - T_i)$; $w_0$ and $w_1$ are the relative masses corresponding to the ignition temperature and burnout temperature, respectively.

**1.3 Kinetic analyses**

To study the reaction mechanism of SS and BC co-combustion, it is necessary to study the reaction kinetics effect of SS and BC to provide guidance for its pyrolysis and combustion [8-10].

The fuel is pyrolyzed in a TG analyzer, and the reaction can be shown as follows:

$$\mathrm{A(s)} \longrightarrow \mathrm{B(s) + C(g)} \quad \text{(S5)}$$

where A represents a solid reactant; B represents the solid phase of pyrolysis reaction products; and C represents the pyrolysis gas generated by the reaction, mainly including $H_2$, CO, $CH_4$, and other noncondensable gases, and generally refers

to gaseous condensable organic macromolecules.

The pyrolysis reaction rate is a function of reaction temperature, heating rate, and mass of reactants, where α represents the conversion rate, $\alpha = (m_0 - m_i)/(m_0 - m_\infty)$, $m_0$, $m_i$, and $m_\infty$ represent the mass of reactants at the initial time, i time, and termination, respectively (kg).

Pyrolysis reaction rate:

$$\frac{d\alpha}{dt} = kf(\alpha) \tag{S6}$$

By combining the Arrhenius formula and reaction rate formula, the integral form of pyrolysis rate can be obtained as follows:

$$\frac{d\alpha}{dt} = Ae^{-\frac{E}{RT}}f(\alpha) \tag{S7}$$

where k is the reaction rate constant ($s^{-1}$), A is the prefactor ($s^{-1}$), E is the activation energy (kJ/mol), R is the gas constant (8.314 J/(mol•K)), T is the temperature (°C), and F(α) is the differential form of the pyrolysis mechanism function.

he early studies on thermal analysis dynamics were all based on isothermal method, and then due to the development of thermal analysis technology, nonisothermal dynamic method gradually replaced the isothermal method with its advantages of rapid and accurate analysis [11,12]. Nonisothermal method usually uses the constant rate of heating, i.e., the heating rate is a constant. Therefore, the decomposition rate of samples determined by nonisothermal dynamics method can be expressed as follows:

$$\frac{\mathrm{d}\alpha}{\mathrm{f}(\alpha)} = \frac{A}{\beta}\mathrm{e}^{-\frac{E}{RT}}\mathrm{d}T \tag{S8}$$

where β is the heating rate (K/min), expressed as β = dT/dt.

According to the Coats–Redfern method, integration by parts can be obtained as follows:

$$\ln\frac{G(\alpha)}{T^2} = \ln[\frac{\mathrm{AR}}{\beta\mathrm{E}}(1-\frac{2\mathrm{RT}}{\mathrm{E}})] - \frac{E}{RT} \tag{S9}$$

Among them $G(\alpha) = \int_0^\alpha \frac{\mathrm{d}\alpha}{\mathrm{f}(\alpha)}$, for most of the reaction E values within the general temperature range, 2(RT)/E is far less than 1, so it can be translated into:

$$\ln\frac{G(\alpha)}{T^2} = \ln\frac{\mathrm{AR}}{\beta\mathrm{E}} - \frac{E}{RT} \tag{S10}$$

At this point, $\ln[\mathrm{G}(\alpha)\cdot\mathrm{T}^{-2}]$ has a linear relationship with $\mathrm{T}^{-1}$ under constant heating rate β, and the slope of fitting data can be used to obtain the apparent activation energy E. Finally, the most reasonable mechanism equation was obtained by comparing the fitting degree of curves under different mechanism functions [13]. The commonly used mechanism functions are listed as the **Table S1**.

**Table S1** Common reaction mechanism functions

| No. | mechanism | G（α） | f（α） |
|---|---|---|---|
| 1 | One-dimensional diffusion，1D | $\alpha^2$ | $1/(2\alpha)$ |
| 2 | Two-dimensional diffusion，2D | $\alpha+(1-\alpha)\ln(1-\alpha)$ | $[-\ln(1-\alpha)]-1$ |
| 3 | Two-dimensional diffusion，2D，n=1/2 | $[1-(1-\alpha)^{1/2}]^{1/2}$ | $4(1-\alpha)^{1/2}[1-(1-\alpha)^{1/2}]^{1/2}$ |
| 4 | Two-dimensional diffusion，2D，n=2 | $[1-(1-\alpha)^{1/2}]^2$ | $(1-\alpha)^{1/2}[1-(1-\alpha)^{1/2}]^{-1}$ |
| 5 | Three-dimensional diffusion，3D，n=2 | $[1-(1-\alpha)^{1/3}]^{1/2}$ | $6(1-\alpha)^{2/3}[1-(1-\alpha)^{1/3}]^{1/2}$ |
| 6 | Three-dimensional diffusion，3D，Spherical symmetry | $[1-(1-\alpha)^{1/3}]^2$ | $3/2(1-\alpha)^{2/3}[1-(1-\alpha)^{1/3}]^{-1}$ |
| 7 | Three-dimensional diffusion，3D，Cylindrical symmetry | $(1-2\alpha/3)-(1-\alpha)^{2/3}$ | $3/2[(1-\alpha)^{-1/3}-1]^{-1}$ |
| 8 | Three-dimensional diffusion，3D | $[(1+\alpha)^{1/3}-1]^2$ | $3/2(1+\alpha)^{2/3}[(1+\alpha)^{1/3}-1]^{-1}$ |
| 9 | Three-dimensional diffusion，3D | $[(1-\alpha)^{-1/3}-1]^2$ | $3/2(1-\alpha)^{4//3}[(1-\alpha)^{1/3}-1]^{-1}$ |
| 10~20 | Random nucleation growth (n=4,3,5/2,2,3/2,4/3，1,2/3,1/2,1/3,1/4) | $[-\ln(1-\alpha)]^{1/n}$ | $1/n(1-\alpha)[-\ln(1-\alpha)]^{(n-1)/n}$ |
| 21 | Autocatalytic reaction，unciform nucleation | $\ln[\alpha/(1-\alpha)]$ | $\alpha/(1-\alpha)$ |
| 22~26 | Power function rule，exponential nucleation | $\alpha^{1/n}$ | $1/n(1-\alpha)^{(n-1)/n}$ |

| | | | |
|---|---|---|---|
| | (n=2/3,1,2,3,4) | | |
| 27 | Geometry of contraction (spherical symmetry), n=1/3 | $1-(1-\alpha)^{1/3}$ | $3(1-\alpha)^{2/3}$ |
| 28 | Geometry of contraction (cylindrically symmetric)，n=1/2 | $1-(1-\alpha)^{1/2}$ | $2(1-\alpha)^{1/2}$ |
| 29 | Chemical reaction order，n=1/4 | $1-(1-\alpha)^{1/4}$ | $4(1-\alpha)^{3/4}$ |
| 30 | Chemical reaction order，n=2 | $1-(1-\alpha)^{2}$ | $4(1-\alpha)^{-1}$ |
| 31 | Chemical reaction order，n=3 | $1-(1-\alpha)^{3}$ | $4(1-\alpha)^{-2}$ |

**Table S2** Types of bonds and typical wavenumber values during the Fourier transform infrared (FTIR) spectrometer process

| Types of bonds | Wavenumber($cm^{-1}$) |
|---|---|
| C-H | 3300 (alkyne stretch) |
| | 3000–2850 (alkanes stretch) |
| | 900–690 (aromatic out-of-plane bend) |
| | 1000–650 (alkenes out-of-plane bend) |
| | 1450–1375 (alkanes: $-CH_3$ bend) |
| | 1465 (alkanes $-CH_2-$ bend) |
| | 3100–3000 (alkenes stretch) |
| C=C | 2900–2800 (aldehyde) |
| | 1680–1600 (alkene) |
| | 1600–1475 (aromatic) |
| C≡C | 2250–2100 (alkyne) |
| C-O | 1300–1000 (alcohol, ethers, esters, carboxylic acids, anhydrides) |
| N-H | 3500–3100 (primary, secondary amines, and amides: stretch) |
| | 1640–1550 (primary, secondary amines, and amides: bend) |
| O-H | 3650–3600 (free alcohols, phenols) |
| | 3400–3200 (H-bonded alcohols, phenols) |
| | 3400–2400 (carboxylic acid) |
| C=O | 1740–1720 (aldehyde) |
| | 1725–1705 (ketone) |

| | |
|---|---|
| | 1750–1730 (ester) |
| | 1725–1700 (carboxylic acid) |
| | 1810–760 (anhydride) |
| | 1680–1630 (amide) |
| | 1800 (acid chloride) |
| C=S | 1168 (thiocarbonyl) |
| S=O | 1033 & 1054 (sulfoxide) |
| N-O | 931 & 965 (aliphatic) |

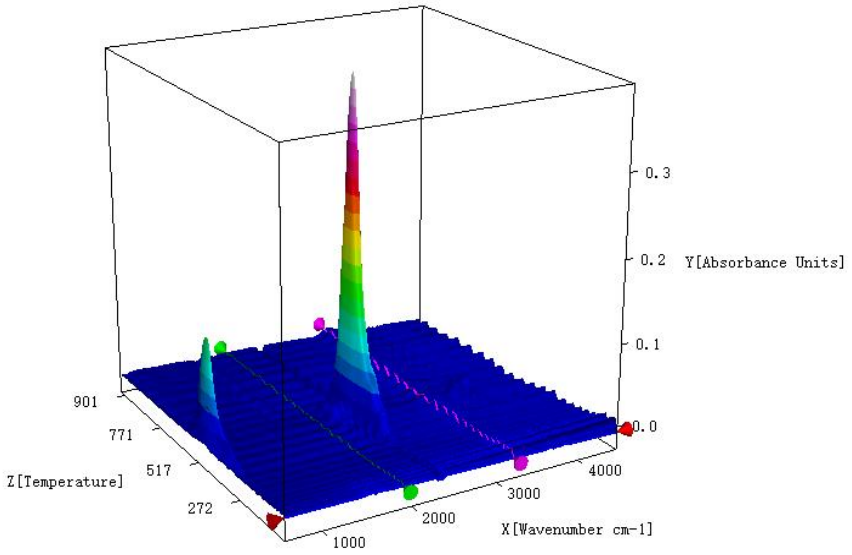


**Figure S1** 3-Dprofiles of FTIR spectra of evolved gases for volatiles with different temperatures during combustion process of BC

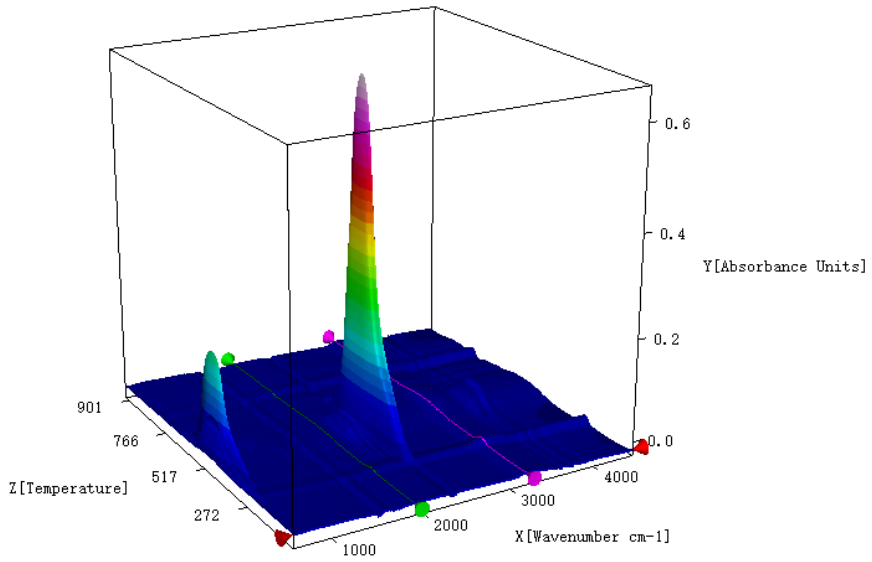


**Figure S2** 3-Dprofiles of FTIR spectra of evolved gases for volatiles with different temperatures during combustion process of SS-50-BC95

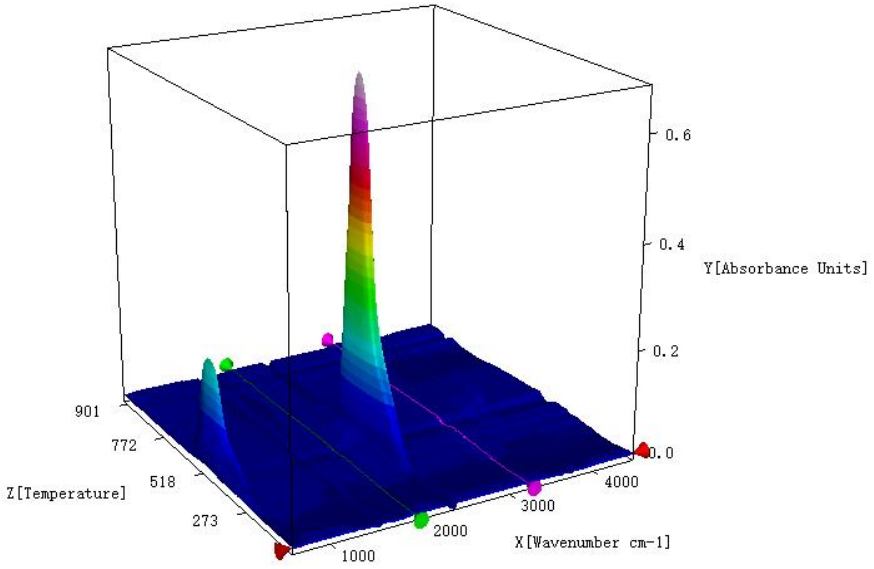


**Figure S3** 3-Dprofiles of FTIR spectra of evolved gases for volatiles with different temperatures during combustion process of SS-50-BC90

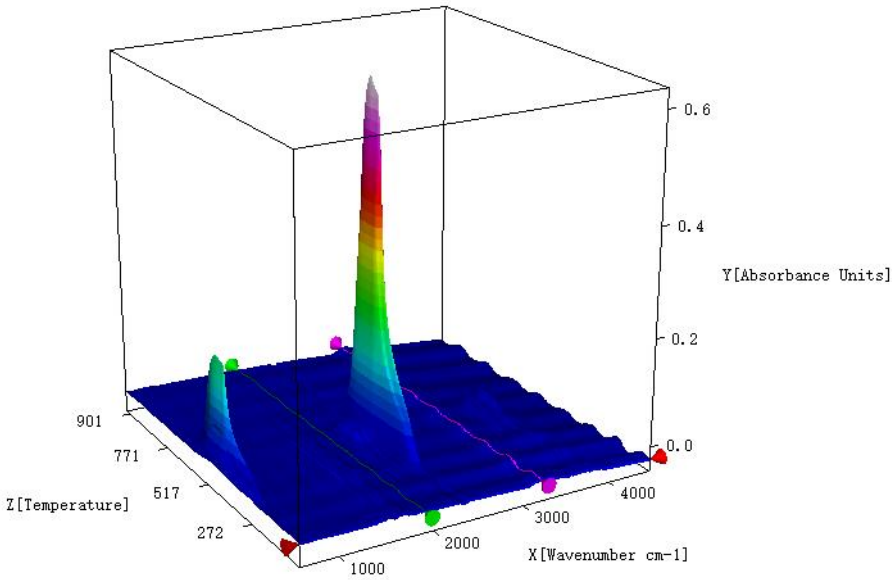


**Figure S4** 3-Dprofiles of FTIR spectra of evolved gases for volatiles with different temperatures during combustion process of SS-50-BC85

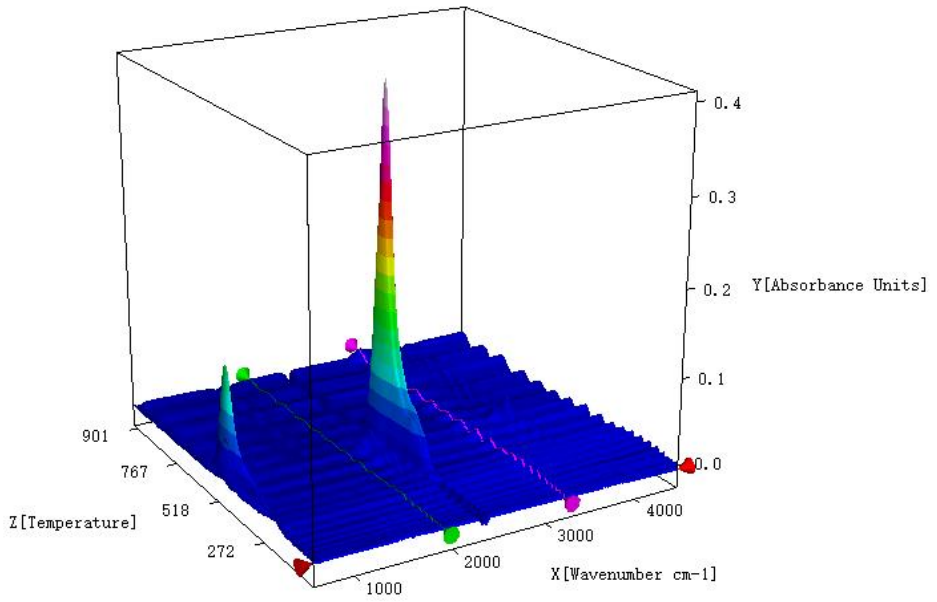


**Figure S5** 3-Dprofiles of FTIR spectra of evolved gases for volatiles with different temperatures during combustion process of SS-50-BC80

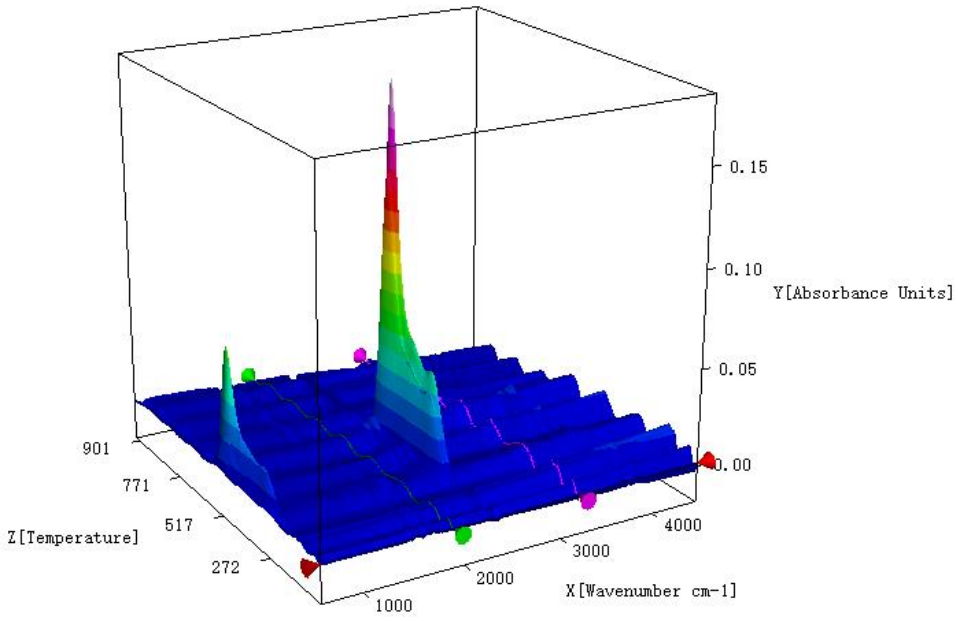


**Figure S6** 3-Dprofiles of FTIR spectra of evolved gases for volatiles with different temperatures during combustion process of SS-50-BC70

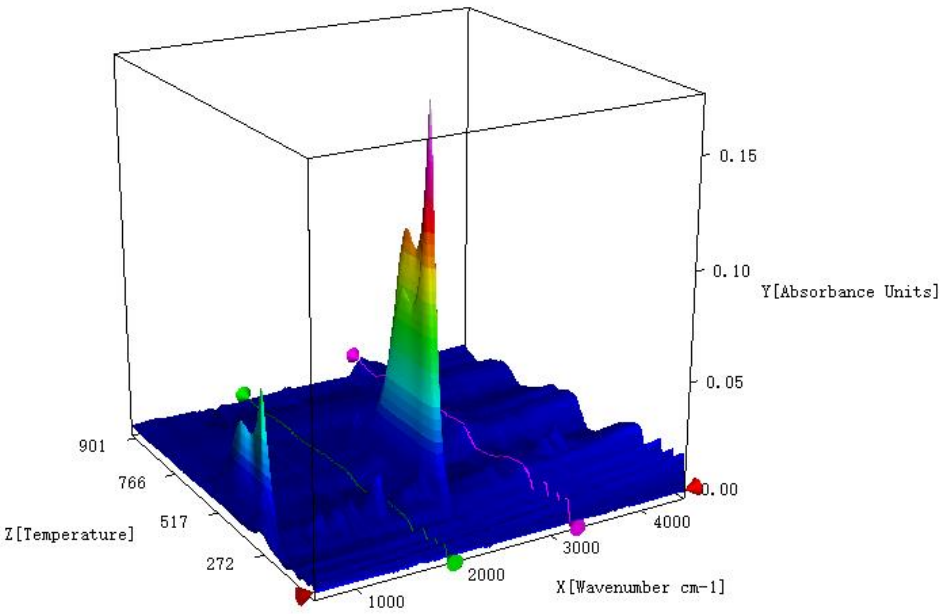


**Figure S7** 3-Dprofiles of FTIR spectra of evolved gases for volatiles with different temperatures during combustion process of SS-50-BC40

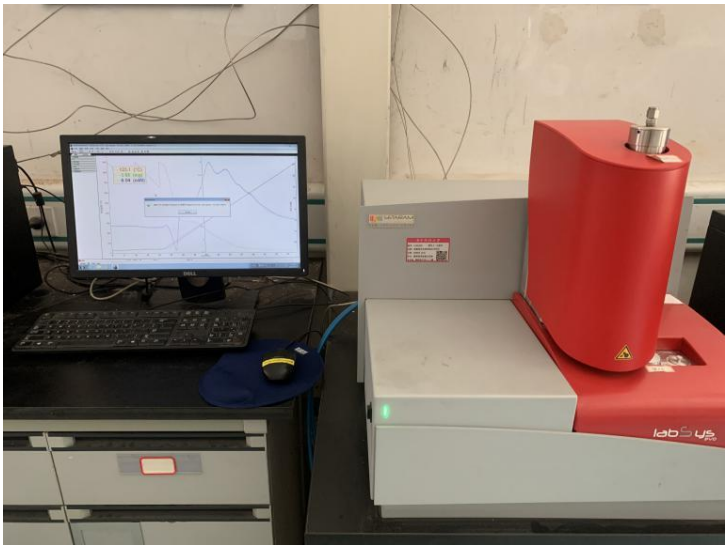

**Figure S8** TG analyzer (Evo1150, Setaram, France)

**Figure S9** The thermogravimetric analyzer (Sta 449F3, Netzsch, Germany) coupled to an FTIR spectrometer (Vertex80v, Bruker, Germany)

**References**


1. Gómez, C.J.; Mészáros, E.; Jakab, E.; Velo, E.; Puigjaner, L. Thermogravimetry/mass spectrometry study of woody residues and an herbaceous biomass crop using PCA techniques. Journal of Analytical and Applied Pyrolysis 2007, 80, 416-426, doi:10.1016/j.jaap.2007.05.003.
2. Zhai, Y.; Peng, W.; Zeng, G.; Fu, Z.; Lan, Y.; Chen, H.; Wang, C.; Fan, X. Pyrolysis characteristics and kinetics of sewage sludge for different sizes and heating rates. Journal of Thermal Analysis and Calorimetry 2011, 107, 1015-1022, doi:10.1007/s10973-011-1644-0.
3. Wang, C.; Wang, F.; Yang, Q.; Liang, R. Thermogravimetric studies of the behavior of wheat straw with added coal during combustion. Biomass and Bioenergy 2009, 33, 50-56, doi:10.1016/j.biombioe.2008.04.013.
4. Li, P.; You, F.; Zhou, H.; Wang, W.; Zhu, Z. On the spontaneous combustion and the thermal stability properties of the coal-based activated carbon powders. Journal of Safety and Environment 2017, 17, 435-439.
5. Liu, Z.; Zhang, J. STUDY ON THE COMBUSTION CHARACTERISTICS AND KINETICS OF Caragana korshinskii Kom. Acta Energiae Solaris Sinica 2017, 38, 2611-2618.
6. Xian, X.; Du, Y.; Zhang, G. COMBUSTION CHARACTERISTICS OF COAL BLENDING BY TG-DTG/DTA. Coal Conversion 2011, 34, 67-70.
7. Yu, L.J.; Wang, S.; Jiang, X.M.; Wang, N.; Zhang, C.Q. Thermal analysis

studies on combustion characteristics of seaweed. Journal of Thermal Analysis and Calorimetry 2008, 93, 611-617, doi:10.1007/s10973-007-8274-6.

8. Magdziarz, A.; Wilk, M. Thermal characteristics of the combustion process of biomass and sewage sludge. Journal of Thermal Analysis and Calorimetry 2013, 114, 519-529, doi:10.1007/s10973-012-2933-y.

9. Iscan, A.G.; Kok, M.V.; Bagci, A.S. Kinetic analysis of central anatolia oil shale by combustion cell experiments. Journal of Thermal Analysis and Calorimetry 2007, 88, 653-656, doi:10.1007/s10973-006-8026-z.

10. Fang, S.; Yu, Z.; Lin, Y.; Lin, Y.; Fan, Y.; Liao, Y.; Ma, X. Effects of additives on the co-pyrolysis of municipal solid waste and paper sludge by using thermogravimetric analysis. Bioresour Technol 2016, 209, 265-272, doi:10.1016/j.biortech.2016.03.027.

11. Starink, M.J. The determination of activation energy from linear heating rate experiments: a comparison of the accuracy of isoconversion methods. Thermochimica Acta 2003, 404, 163-176, doi:10.1016/s0040-6031(03)00144-8.

12. Sima-Ella, E.; Yuan, G.; Mays, T. A simple kinetic analysis to determine the intrinsic reactivity of coal chars. Fuel 2005, 84, 1920-1925, doi:10.1016/j.fuel.2005.03.022.

13. Yang, K.; Ding, Z.J.; Xiao, L.C.; Li, Q. Pyrolysis Characteristics and Kinetic Analysis of Municipal Sewage Sludge Coupled with Sawdust. Reneng Dongli Gongcheng/Journal of Engineering for Thermal Energy and Power 2018, 33,

112-118, doi:10.16146/j.cnki.rndlgc.2018.03.017.